Peer reviewed version

Link to published version (if available):
10.1016/j.actamat.2015.09.045

Link to publication record in Explore Bristol Research
PDF-document

University of Bristol - Explore Bristol Research
General rights

Control of the in-plane thermal conductivity of ultra-thin nanocrystalline diamond films through the grain and grain boundary properties.

Julian Anaya[a,*], Stefano Rossi[b], Mohammed Alomari[b], Erhard Kohn[b], Lajos Tóth[c], Béla Pécz[c], Karl D. Hobart[d], Travis J. Anderson[d], Tatyana I. Feygelson[d], Bradford B. Pate[d], Martin Kuball[a]

[a]*Center for Device Thermography and Reliability, University of Bristol.*
[b]*Institute of Electron Devices and Circuits (EBS), Ulm University, Ulm, Germany.*
[c]*Centre for Energy Research, Institute for Technical Physics and Materials Science, Budapest, Hungary.*
[d]*Naval Research Laboratory, Washington DC 20375.*

Abstract

The in-plane thermal conductivity of polycrystalline diamond near its nucleation site, which is a key parameter to an efficient integration of diamond in modern high power AlGaN/GaN high electron mobility devices, has been studied. By controlling the lateral grain size evolution through the diamond growth conditions it has been possible to increase the in-plane thermal conductivity of the polycrystalline diamond film for a given thickness. Besides, the in-plane thermal conductivity has been found strongly inhomogeneous across the diamond films, being also possible to control this inhomogeneity by the growth conditions. The experimental results has been explained through a combined effect of the phonon mean free path confinement due the grain size and the quality of the grain/grain interfaces, showing that both effects evolve with the grain expansion and are dependant on the diamond growth conditions. This analysis shows how the thermal transport in the near nucleation region of polycrystalline diamond can be controlled, which ultimately opens the door to create ultra-thin layers with a engineered thermal conductivity, ranging from a few W/mK to a few hundreds of W/mK.

---

*Corresponding author
Email address:* `J.anayaCalvo@bristol.ac.uk` (Julian Anaya)

1. Introduction:

Recently, the integration of diamond with high power AlGaN/GaN high mobility electron devices (HEMTs) was demonstrated to be a very promising solution to optimize their heat management,[1, 2, 3, 4, 5, 6, 7, 8, 9, 10] which enables handling much higher operational electrical power densities.[1] To take full advantage of the high thermal conductivity of diamond, reaching up to 3000 W/mK for single crystalline high quality diamond, the diamond heat dissipation layer should be located as close as possible to the heat source, ie the device channel.[4, 8] This is achieved by directly growing diamond films on the devices, which results in polycrystalline diamond films rather than single crystal diamond. However, while the thermal conductivity of polycrystalline diamond may reach values close to that of the single crystal diamond,[11] the thermal transport near its near nucleation site may be much lower due the small grain size and the accumulation of defects in this region.[12, 13] Two strategies for combining diamond with the devices using the direct growth approach have emerged in the recent years, , namely, either by substituting the SiC or Si substrate,[1, 3, 4, 5] or by growing the diamond films on top of the device passivation layer.[6, 7, 8, 9, 10] However, in both strategies the heat has to diffuse across the nucleation region of the diamond film, and therefore knowing how the heat is spread in the first microns of the polycrystalline diamond is fundamental in order to optimize their thermal resistance and thus improve their lifetime and reduce its energy consumption. A few inconsistent results are available in the literature about the in-plane thermal transport in the first microns of polycrystalline diamond showing values ranging from a few W/mK up to 800 W/mK for layers thicknesses below 2 μm.[13, 14, 15, 16, 17, 18, 19, 20, 21, 22, 23, 24] Also a strong inhomogeneity of the in-plane thermal conductivity through the diamond films has been reported,[11, 12, 21, 22, 24] although mostly for films larger

2

than a few micrometer thickness, due to challenges in measuring the thermal properties of very thin diamond films. Therefore a clear description of the heat transport in the complex near nucleation region of polycrystalline diamond is still lacking. In this paper, we study the in-plane thermal transport in the near nucleation region of polycrystalline diamond, which consist on nanocrystalline diamond (NCD), through a set of controlled ultrathin diamond films of different thickness, grain sizes and growth methods, with its thermal conductivity being determined with a direct steady-state technique developed recently. [24] This enables the correlation between the lateral heat transport and the physical properties of the samples, namely thickness and grain sizes. The results can be explained through a theoretical model which takes into account the effect of the grain size in terms of shortening of the phonon mean free path and also the temperature gradients in the defective grain boundaries. This analysis allows the characterization of the quality of the grain/grain interfaces and also explains the inhomogeneous in-plane thermal conductivity observed in ultra-thin diamond films.

2. Experimental Details:

NCD films were grown on single crystal Si<100> wafers using two different strategies, hot filament chemical vapor deposition (HF-NCD) and microwave plasma chemical vapor deposition (MW-NCD). The deposition of the NCD film on a foreign substrate is a 2 steps process consisting on a nucleation phase, followed by an overgrowth stage. The HF-NCD samples were nucleated under similar conditions to the ones described in ref [25] by bias enhanced nucleation (BEN) performed in-situ in the same reactor used for the overgrowth, resulting in crystallite densities of more than 10^{10} cm^2. For the MW-NCD samples the seeding process described in ref [26] was used to form the nucleation layer. For this, Si wafers were first sonicated in a nanodiamond-ethanol solution for 30 minutes; and then in pure ethanol to remove all non-adherent diamond seeds. The seeding solution is a suspension of detonation nanodiamond, with an av-

erage grain size of 4-6nm. Next, wafers are placed in a spin tool where they are spray-rinsed and dried. This seeding method typically achieves uniform nucleation with a density exceeding 10^{12} cm^{-2}. After the nucleation, the grain evolution of diamond may be controlled during the overgrowth phase by varying the concentration of methane in the hydrogen carrier gas (CH$_4$/H$_2$), the temperature of the substrate (T$_{subs}$) and the pressure of the CVD chamber. [27, 28, 29] Two sets of growth conditions at 1.5 kPa were used to grow the HF-NCD films of different thicknesses: 470, 680 and 1000 nm using 0.4% CH$_4$/H$_2$, and a T$_{subs}$ of 750 ^{o}C (recipe A) and 480, 860, 980 and 1500 nm with 0.2% CH$_4$/H$_2$, and T$_{subs}$=825°C (recipe B). The two growth conditions were chosen to produce a different lateral grain evolution, resulting in different grain sizes for a given thickness, illustrated in the scanning electron microscopy (SEM) micrographs in Fig. 1 a). Note that samples grown with Recipe B exhibit faster lateral grain expansion (see Fig.1). The average in-plane grain size on the top of the diamond films was determined from the SEM micrographs using the three-circle procedure proposed by Abrams for polycrystalline materials, [30] with the results shown in Fig. 1-b). Note that for the two HF-NCD recipes the lateral grain size follows a linear relationship with thickness, with the slope for the recipe B faster than the one for recipe A. This lateral expansion holds within the first 1000nm, while thereafter the grain size lateral expansion is lowered (see Fig 1-b. sketch). To test the general applicability of the results and model obtained here through HF-diamond in a broader field, the results were compared to similar MW-diamond grown at a substrate temperature of 750 ^{o}C with a CH$_4$/H$_2$ ratio of 0.5 and 0.33 for recipes 1 and 2, respectively. Such conditions yield a similar lateral grain size at 1μm as the HF-NCD recipes A and B respectively (Fig 1 b).

For measuring the in-plane thermal conductivity of these ultra-thin NCD films, we applied a technique described in reference [24] which is based on Raman thermography assisted by Silicon nanowires acting as surface nano thermometers. For measuring Raman spectra a Renishaw InVia spectrometer with an Ar+ 488 nm laser line was used. A lateral resolution better than 1 μm

4

was obtained by using the confocal mode with a 50 X 0.65 NA objective. Free standing membranes were created in the samples by selectively etching away the silicon substrate underneath the diamond. Etching of the Si substrate was accomplished both by a wet-etch (MW-NCD) and by a dry-etch process (HF NCD). In the former, the etching was performed by dipping the sample into a KOH solution while for the dry-etch process, etching was performed in a inductively coupled plasma (ICP) reactor by means of SF_6/C_4F_8 gases; for this a etch-mask of 300 nm thick Al film was used. On top of the freestanding membranes, 5 μm wide thin metal stripe (Ti/Au) was deposited in the center of the freestanding membrane to act as a heating source. When a current flows through the metal stripe, the Joule heating results in heat which flows into the diamond and laterally along the membrane, and ultimately into the Si substrate. Silicon NWs were also deposited on top of the membranes and metal surface providing an accurate local peak temperature measurement. From the temperature profiles measured from the heater to the edge of the substrate, lateral thermal conductivity can be extracted by solving the Heat equation. Temperature was measured in the diamond membrane and from the silicon NWs by means of Raman thermography, based on the phonon frequency shift as function of temperature as described in reference [24].

3. Experimental Results:

Fig. 2 shows an example of a temperature profile obtained from the diamond membranes for the 470 nm thick HF-NCD of recipe B, and corresponding temperature profiles are obtained for the other investigated samples. The determined in-plane thermal conductivity of each as-grown NCD layer is shown in Fig. 3. The thermal conductivity values are in general one to two orders of magnitude below the thermal conductivities reported for bulk CVD diamond for all the investigated samples.[11] Both families of HF NCD samples show a linear correlation with its layer thickness (see Fig 3 A).We also noted that the slope of the temperature profiles used to determine the thermal conductivity

5

can be fitted assuming a temperature independent in-plane thermal conductivity. In bulk diamond, and above room temperature, it is well known that the thermal conductivity decreases with temperature due to the 3 phonon scattering mechanism,[31] being this decay well reproduced by a power law given as $k(T) = k_{300K}(T/300K)^{-1.25}$ extracted from the fitting to the experimental data of reference. [32] However, when such temperature dependence is assumed for the NCD membranes it is not possible to simultaneously reproduce the experimental temperature profiles for different powers dissipated in the heater (see Fig. 2). This deviation from the bulk behavior of the phonon transport indicates that the in-grain phonon phonon scattering in the near nucleation site of the NCD membranes is not the dominant phonon scattering mechanism in these samples from room temperature and above, being the dominant phonon scattering mechanism either due to the phonon scattering at the grain boundaries or the phonon scattering due defects/impurities in the lattice.

The thermal conductivity of samples of recipe B are higher than those samples grown with recipe A, due to the different evolution of the grain size (Fig 1-b). The results obtained for the MW NCD samples are consistent with the HF-NCD. The importance of the grain size for thermal conductivity is highlighted in Fig 3-b, where the in-plane thermal conductivity as function of the average grain size measured at the surface of the diamond films is displayed. Independent of growth recipe, thickness and growth method a nearly linear correlation between the in-plane thermal conductivity and the average grain size is observed. These results illustrate that as a thumb rule the as-grown NCD samples with a faster lateral grain size evolution will achieve a higher lateral thermal conductivity for a given thickness than NCD films with lower grain size evolution rate. This ultimately opens a door to manipulate the thermal properties of the near nucleation region of polycrystalline diamond by acting on the grain evolution through the growth conditions.

To gain insight into the changes in thermal conductivity through the layer thickness, we took advantage of the stepwise growth of the HF-NCD series of samples by analyzing the results through a recursive multilayer model.[24] For

6

this we started with a layer with a thickness d_n, corresponding to the thinnest sample available in the set, with k_n its experimentally determined thermal conductivity. On top of this layer, and assuming continuity as boundary condition, a second layer of thickness d' is considered to match the total thickness of the next sample of the set. Therefore the temperature profile experimentally measured in this sample should be reproduced by a two layer model in which the only unknown parameter is the thermal conductivity of the top layer, k_{n-1}. This can be done recursively for as many layers as samples are available, and provides an evaluation of how the in-plane thermal conductivity changes through the layer thickness. The results of the recursive multilayer model for the HF NCD are summarized in Fig 4, showing that the thermal conductivity is strongly inhomogeneous across the layer thickness, varying up to a factor 3 between the first 500 nm (near the nucleation layer) and the top part of the film. It is worth noting that the depth-dependence of the in-plane thermal conductivity is stronger in the sample grown with the recipe A, which is not consistent with a simple grain size dependence and indicates that the lateral grain size is not the only factor in the reduction of the in-plane thermal conductivity observed in the NCD films.

To extend the validity of the stepwise experimental approach, membranes were etched from the nucleation site to remove the first 420 nm of diamond. This enabled a direct measurement of the in-plane thermal conductivity of the top part of the diamond film, in this case of the MW NCD layers for which no stepwise set of samples were available. The temperature profile measured in the thinned membranes, when the same power was dissipated into the metal heaters, was found equivalent to the original thicker as-grown membranes. Given that the power density inside the NCD layer is almost doubled due the thinning of the sample, this indicates a clear improvement in the measured thermal conductivity after the etching (see Fig. 5-a). In-plane thermal conductivities of 120 ± 5 W/mK for sample 1 (80W/mK before etching) and 175 ± 5 W/mK for sample 2 (135 W/mK before etching) were measured from the etched samples. Using the same recursive model described before, but in a reverse direction, the thermal conductivity of the near nucleation etched part was also extracted, shown in

7

Fig. 5-b. MW NCD and HF NCD equivalent membranes show a very similar variation of the in-plane thermal conductivity across the layer, consistent with a similar grain evolution for both sets of samples even with the different processes used to grown each set of samples.

4. Discussion:

Modeling the thermal transport of complex NCD is a challenging task involving the evaluation of the different thermal resistances in the diamond lattice, namely the thermal resistance inside the grains and the thermal resistance between grains. The intrinsic thermal conductivity for dielectrics and semiconductors can be modeled by solving the Boltzmann transport equation for the phonons in the lattice (BTE).[33] However, here the approach given by Callaway was used to circumvent the exact solution of the complex multidimensional BTE for phonons.[34, 35, 36] This formalism was derived as a phenomenological model for low temperatures where the three phonon scattering events which conserve the wave vector (Normal process) and those who do not (resistive phonon scattering processes) contribute to the total thermal resistance and it has been extended to the full temperature range by considering the different acoustic phonon polarizations and accurate scattering relaxation times.[35, 36, 37, 38] Following this formalism the thermal conductivity can be modeled as follows:

$$k = \frac{T^3 K_B^4}{8\pi^3 \hbar^3} \sum_i \frac{1}{v_i} [I_1^i + \beta^i \times I_2^i] \tag{1}$$

where the thermal conductivity of the first term I_1^i is equivalent to diffusive phonon thermal transport and the second term I_2^i, modified by the relaxation time β^i takes into account the drift in the phonon distribution introduced by the Normal 3-phonon scattering processes.[36, 39] The different polarizations of the phonons, i, were taken into account by using the Holland modification to the Callaway model.[35, 36] The two terms I_1^i and I_2^i are described by:

8

$$I_1^i = \int_0^{2\pi} \int_0^{\pi} \int_0^{\theta^i/T} \tau_C^i \times \frac{x^4 e^x}{(e^x - 1)^2} \cos^2 \theta \sin \theta \, dx d\theta d\phi \ ,$$

$$I_2^i = \int_0^{2\pi} \int_0^{\pi} \int_0^{\theta^i/T} \frac{\tau_C^i}{\tau_N^i} \times \frac{x^4 e^x}{(e^x - 1)^2} \cos^2 \theta \sin \theta \, dx d\theta d\phi$$

$$(2)$$

with θ_i being the temperature cut-off of each phonon branch i, τ_N^i the Normal 3-phonon scattering relaxation time and $\tau_C^i = (\frac{1}{\tau_N^i} + \frac{1}{\tau_R^i})^{-1}$ a combination of the Normal ans resistive scattering processes.[34] Here the Normal 3-phonon processes are assumed to behave following the relaxation times given by Asen-Palmer:[37]

$$\tau_N^L = \frac{1}{C_N^L \omega^2 T^3}$$

$$\tau_N^T = \frac{1}{C_N^T \omega T^4}$$

$$(3)$$

For the resistive processes, which are given as a combined relaxation time following a Mathiesen rule, being the umklapp 3 phonon processes given as: [38]

$$\tau_U^i = \frac{1}{C_U^i \omega^2 T e^{\theta_i/3T}}$$

$$(4)$$

and the scattering introduced by the impurities/isotopes is given in the Klemens formalism as: [40]

$$\tau_I^i = \frac{1}{C_I^i \omega^4 \Gamma}$$

$$(5)$$

The constants C_j^i appearing in (3) (4) and (5) depend only on the properties of the material and are fully described for diamond by Morelli et al. in Ref [[38]]. Here to simplify the model, we encompassed the effect of the different factors descriving the quality of the lattice (different isotopes, vacancies, impurities and extended defects) in the parameter Γ whitout distinction, which is a sensible approach since from room temperature and above all these mechanisms can be descrived by (5).[40] Finally, the effect of the finite size of the lattice might be introduced into τ_R^i through a simple time constant proportional to the phonon

sound velocity of each branch and the effective length of the boundary,L_{eff} : [33]

$$\tau^i_{B/GB} = \frac{L_{eff}}{v_i} \qquad (6)$$

With this model, the thermal conductivity of bulk single crystal natural diamond has been reproduced with high accuracy in a wide range of tempera-

225 tures in the past. [38] Furthermore, it has been successfully applied to describe the thermal conductivity of polycrystalline dielectrics by simply assuming L_{eff} as the lateral dimension of the grains [11, 41, 42, 43, 44], and thus considering a near the Casimir limit for the mean free path of the phonons.[33] This holds for diamond since its acoustic phonons carrying the energy have very

230 long phonon mean free paths (MFP), being half of the heat carried by phonons with MFPs above 1 μm at room temperature.[45] Therefore, when the dimensions of the grains are reduced below few microns, the phonons are affected by $\tau^i_{B/GB}$ and the thermal conductivity is reduced. However, it is worth noting that in polycrystalline diamond, the fast lateral growing of the grains, and the

235 competition process between them, can distort the homogenous arrangement of the atoms at the grain boundaries.[46] This ultimately promote the accumulation of vacancy clusters, and other impurities like hydrogen atoms forming C-H bonds,[28, 46, 47, 48, 49, 50] which has been correlated with a reduction in the thermal conductivity of the polycrystalline diamond.[51] The thickness of this

240 defective region between grains depends on the details of the growth,[46] and here a conversion of the propagative acoustic phonon modes in optical modes acting as a energy reservoir can take place.[52] All this together lead to a localized ΔT between grains for which the aforementioned Callaway like model cannot account for.To include the full role played by the grain boundaries, we

245 consider here two different sources of thermal resistance: first the one originating from the reduction of the phonon mean free path due the phonon phonon interactions, impurities in the lattice and the size of the grains, which is described by the Callaway-like model, and secondly a thermal resistance arising

from the localized accumulation of defects at the grain boundaries, in which the heat transference is characterized by a thermal conductance G. This is therefore equivalent to the effective thermal conductivity (ETC) model recently proposed by Dong et al.,[53] but here the size-effect in the intra grain thermal conductivity is described by $\tau_{B/GB}^i$ inside the Callaway like model instead from the phenomenological approach of the original ETC model.[53] Under this approach the model describing the thermal transport in polycrystalline diamond is given as:

$$k^{KC}(G, \Gamma, L_{eff}, T) = \frac{k(\Gamma, L_{eff}, T)}{1 + \frac{k(\Gamma, L^{eff}, T)}{L_{eff} \times G}} \tag{7}$$

where $k(G, \Gamma, L_{eff}, T)$ is the thermal conductivity calculated with the Callaway-like model including the size effects through $\tau_{B/GB}^i$ and G takes account of the extra thermal resistance between grains due the defect accumulation at the boundary between grains. It is worth noting that in a more detailed picture of the phonon transport, both $\tau_{B/GB}^i$ and G are likely to have a frequency dependence.[54] However, this frequency dependence is important mainly at low temperatures in which the heat is carried mainly by phonons with long wavelengths, which are more affected by the grain/grain interfaces.[55] Therefore, for room temperature and above, assuming a frequency independent behavior for both $\tau_{B/GB}^i$ and G is a sensible approach which enables to quantify the effect of the grain/grain interfaces in the thermal transport of nanocrystalline diamond. The model described here compares well with ab-initio predictions made by molecular dynamics for nanocrystalline diamond, and also with the ones from the phenomenological ETC model of Ref [[53]] (Fig 6-a). However, the analytical description of the in-grain thermal conductivity introduced here also includes the effect of the lattice defects and the temperature dependence of the thermal conductivity, contributions which are neglected in the original ETC model in the analysis of the thermal transport of polycrystalline materials. To better illustrate the relative importance of the grain size and the quality of the lattice on the in-plane thermal conduc-

tivity of polycrystalline diamond, we show in Fig 6-b a summary of experimental in-plane thermal conductivities versus grain size from the literature (room temperature thermal conductivity and grain size measured from the surface).[11, 13, 14, 15, 16, 17, 56, 57, 58, 59, 60, 61, 62, 63, 64, 65, 66, 67, 68] Note that for crystal sizes below a few tens of nanometers the thermal conductivity decreases up to 3 orders of magnitude from the bulk values, as illustrated in Fig 6-a. Also, it is clear that the data shown in Fig 6-b cannot be explained only with the grain size of the samples. Using only the Callaway like model (thus $G=\infty$ on (7)), the thermal conductivity of the CVD diamond with grains above one micron can be reproduced fairly well only by adjusting the strength of the impurity scattering Γ; however an equivalent of 2500 ppm of carbon vacancies in the lattice would be needed in order to cover the full range of reported thermal conductivities with grains above 1 μm (assuming a Ratsifaritana Klemens behavior for carbon vacancy in Γ [69]). Below this grain size, the strength of Γ should be increased even further to unrealistic values (up to an equivalent of more than 1-2% of carbon vacancies in the lattice) to explain the low thermal conductivity observed for diamond, suggesting that the quality of the lattice is not enough to explain the thermal conductivity observed in nanocrystalline diamond. Only when the thermal resistance between grain is included, the in-plane thermal conductivity of the samples shown in Fig 6-b can be better described, especially the sub 1 μm region which is more sensitive to the grain/grain thermal barrier than to the in grain lattice quality. It is worth noting that for grains bigger than 1 μm the thermal conductivity becomes more sensitive to the quality of the in-grain lattice than by the grain/grain thermal barriers (see Fig 6). And therefore, for the grain size region of the herein investigated samples, which is between 100 nm and 250 nm, the in-plane thermal conductivity will be dominated by the quality of the grain/grain interfaces and the lateral grain size dimensions rather than for the quality of the lattice. Besides, both HF NCD and MW NCD samples showed no signature of non-diamond phases on the Raman spectra, showing also a high transparency (see Fig 2). Typically the optical transparency and thermal conductivity are

12

correlated, being opaque samples prone to accumulate a high density of point defects in the diamond lattice.[70] Also low thermal conductivities due poor lattice quality has been correlated with theCH$_4$/H$_2$ ratio; typically samples grown with more than 1%CH$_4$/H$_2$ show a strong reduction of the thermal conductivity with the CH$_4$/H$_2$ ratio. [13, 71, 72, 73] Since the samples analyzed here are grown with much lowerCH$_4$/H$_2$ ratio than this limit, and their transparency and Raman spectra characteristics, nothing indicates the high point defects needed to impact the thermal conductivity in the grain size range shown by the herein analyzed samples.

For evaluating the in-plane thermal conductivity of the different samples analyzed in this work, the lateral grain size value L_{eff} was estimated from the grain evolution shown in Fig.2 taking advantage of the linear behavior shown in the first micron from nucleation to the surface. For the thicker HF-NCD sample of set B for which the top 500 nm are beyond the linear grain evolution, the lateral grain size of the first micron with the subsequent constant lateral grain size of the top 500 nm of the membrane was averaged. By introducing this effective grain size in the model, a reasonable good agreement with the experimental data is achieved when the grain/grain thermal conductance G is within the 1 GW/m^{2}K to 2 GW/m^{2}K range (see Fig 7-A). These values are lower than those reported for NCD from molecular dynamics simulations (7-8 GW/m^{2}K), however in those simulations the grain/grain interface is created with perfect arrangements of carbon atoms, resulting in an underestimation of the thermal resistances of real samples. The temperature dependence of the in-plane thermal conductivity predicted for this samples is also shown in Fig. 7 (inset). The strong decrease of the thermal conductivity with the temperature which is characteristic of phonon-phonon scattering is suppressed here as a result of the dominant role played by the grain boundaries, yielding an almost constant thermal conductivity above room temperature as we observed in the experimental results (see Fig 2). From Fig. 7, it is also clear that samples showing the fastest grain size expansion (both for HF and MW-NCD) show higher values for G, being all the data contained in the 1.5-2 GW/m^{2}K range, while the

13

samples grown with slower grain evolution lie within a 0.5-1 GW/m^2K band. This indicate that apart from a larger lateral grain size, those HF and MW NCD films exhibiting a faster lateral grain size expansion also have a better grain/grain interface, which ultimately contributes to achieve a higher in-plane thermal conductivity.

The relative contribution of the grain size and grain/grain thermal conductance in the total thermal conductivity of nanocrystalline diamond is shown in Fig-8a. Note Even with the thermal conductance extracted for clean boundaries from ab-initio molecular dynamics ($\sim 7GW/m^2K$), the in-plane thermal conductivity of polycrystalline diamond with crystal sizes below 100 nm is bounded to 250 W/mK. On the other hand, even for relatively big crystals (>250 nanometers), the thermal conductivity can drop below 100 W/mK if the grain/grain interfaces accumulates enough defects or disorder. Finally, to analyze the depth dependence of the in-plane thermal conductivity through the layer thickness observed in the investigated samples, instead of assuming only one average grain size for each membrane, an effective lateral grain size for each region shown in Figs. 4 and 5 may be defined. This again can be approximated from a linear interpolation of the grain evolution data shown in Fig. 2. These results are summarized in Fig 8-b, in which a linear trend is observed for the experimental in-plane thermal conductivities. However this trend is not compatible with a constant value of G across the diamond thickness, suggesting that the thermal conductance between grain/grain interfaces evolves from 0.5 GW/m^2K in the first nanometers up to 3 GW/m^2K above 1 micron diamond growth. Therefore, the distortion of the heat flux because of the grain/grain interface in the first hundreds of nanometers corresponding to the coalescence region is stronger than in the columnar region in which the grains are more homogeneous. This kind of behavior has been shown before in ultrananocrystalline diamond [15], and attributed to the accumulation of defects in the grain/grain boundaries. [15, 50, 68] On the other hand, samples showing slower growth expansion have the worst grain/grain thermal conductance in the near nucleation region, indicating that the growth conditions play a major role in order to achieve a good

14

in-plane thermal conductivity in the near nucleation region. This can be the result of a higher accumulation of defects for the slower diamond growing conditions, but also might be the result of an accumulation of smaller grains than predicted from the linear grain evolution observed above this thickness (see fig 8-a). In any case the strong inhomogeneity observed in the in-plane thermal conductivity across the nanocrystalline membranes is important for the integration of ultra thin diamond layers as a heat spreader, especially if the dimensions of the heat source are much smaller than the thickness of the membrane, or if the frequency of the heating is very high.[6, 8] In those cases the real thermal resistance might be higher than the one expected from the average values determined for the full layer. Also this effect should be considered when the thermal conductivity is measured through transient measurements, being possible to measure difference values for the thermal conductivity of the nanocrystalline diamond when different frequencies, and thus penetration depths, are used for the modulation of the heat source as has been recently experimentally observed by Bozorg-Grayeli et al.[20]

5. Summary:

The thermal conductivity of nanocrystalline diamond on a set of ultrathin diamond membranes was measured. The results illustrate not only that the in-plane thermal conductivity is significantly lower than diamond bulk values, but also that this property can be controlled through its granular nanostructure, being the grain size expansion the key parameter in the process. Thermal conductivity depth profiles were determined with different methods, demonstrating the strong inhomogeneity of the lateral thermal conductivity at different depths inside the NCD diamond; the in-plane thermal conductivity of the first hundreds of nm is much lower than the values achieved in the subsequent columnar region of the diamond film. These results have been explained through a model for the thermal conductivity of polycrystalline materials which takes into account the effect of grain boundary scattering and defect accumulation at the bound-

aries. An extra thermal resistance in the grain boundaries attributed to defect incorporation in these regions has been established, showing that the thermal transport is better in the columnar region in which the grains are more homogeneous in size and worse in the first hundreds of nanometers corresponding to the coalescence region. Given that nowadays it is not known how to grow single crystal ultra-thin CVD diamond layers, the effects described in this work cannot be avoided, and therefore they should be taken into account when diamond is grown as a heat spreader. Furthermore, it has been demonstrated here how the in-plane thermal transport in the near nucleation region of polycrystalline diamond can be controlled, which ultimately opens the door to create thin layers with a desired thermal conductivity, ranging from a few W/mK to a few hundreds of W/mK.

acknowledgments

References

[1] J. Felbinger, M. Chandra, Y. Sun, L. F. Eastman, J. Wasserbauer, F. Faili, D. Babic, D. Francis, F. Ejeckam, Comparison of gan hemts on diamond and sic substrates, Electron Device Letters, IEEE 28 (2007) 948–950.

[2] M. Alomari, A. Dussaigne, D. Martin, N. Grandjean, C. Gaquiere, E. Kohn,

Algan/gan hemt on (111) single crystalline diamond, Electronics Letters 46 (2010) 299–301.

[3] Q. Diduck, J. Felbinger, L. Eastman, D. Francis, J. Wasserbauer, F. Faili, D. Babic, F. Ejeckam, Frequency performance enhancement of algan/gan hemts on diamond, Electronics Letters 45 (2009) 758–759.

[4] J. W. Pomeroy, M. Bernardoni, D. C. Dumka, D. M. Fanning, M. Kuball, Low thermal resistance gan-on-diamond transistors characterized by three-dimensional raman thermography mapping, Applied Physics Letters 104 (2014) –.

[5] J. Cho, Z. Li, E. Bozorg-Grayeli, T. Kodama, D. Francis, F. Ejeckam, F. Faili, M. Asheghi, K. Goodson, Improved thermal interfaces of gan 2013;diamond composite substrates for hemt applications, Components, Packaging and Manufacturing Technology, IEEE Transactions on 3 (2013) 79–85.

[6] M. Tadjer, T. Anderson, K. Hobart, T. Feygelson, J. Caldwell, C. Eddy, F. Kub, J. Butler, B. Pate, J. Melngailis, Reduced self-heating in algan/gan hemts using nanocrystalline diamond heat-spreading films, Electron Device Letters, IEEE 33 (2012) 23–25.

[7] M. Seelmann-Eggebert, P. Meisen, F. Schaudel, P. Koidl, A. Vescan, H. Leier, Heat-spreading diamond films for gan-based high-power transistor devices, Diamond and Related Materials 10 (2001) 744 – 749. 11th European Conference on Diamond, Diamond-like Materials, Carbon Nanotubes, Nitrides and Silicon Carbide.

[8] T. Anderson, A. Koehler, K. Hobart, M. Tadjer, T. Feygelson, J. Hite, B. Pate, F. Kub, C. Eddy, Nanocrystalline diamond-gated algan/gan hemt, Electron Device Letters, IEEE 34 (2013) 1382–1384.

[9] A. Wang, M. J. Tadjer, F. Calle, Simulation of thermal management in

17

algan/gan hemts with integrated diamond heat spreaders, Semiconductor Science and Technology 28 (2013) 055010.

[10] M. Alomari, M. Dipalo, S. Rossi, M.-A. Diforte-Poisson, S. Delage, J.-F. Carlin, N. Grandjean, C. Gaquiere, L. Toth, B. Pecz, E. Kohn, Diamond overgrown inaln/gan {HEMT}, Diamond and Related Materials 20 (2011) 604 – 608.

[11] J. E. Graebner, M. E. Reiss, L. Seibles, T. M. Hartnett, R. P. Miller, C. J. Robinson, Phonon scattering in chemical-vapor-deposited diamond, Phys. Rev. B 50 (1994) 3702–3713.

[12] J. E. Graebner, S. Jin, G. W. Kammlott, J. A. Herb, C. F. Gardinier, Unusually high thermal conductivity in diamond films, Applied Physics Letters 60 (1992) 1576–1578.

[13] K. Plamann, D. Fournier, E. Anger, A. Gicquel, Photothermal examination of the heat diffusion inhomogeneity in diamond films of sub-micron thickness, Diamond and Related Materials 3 (1994) 752 – 756. Proceedings of the 4th European Conference on Diamond, Diamond-like and Related Materials.

[14] B. Lee, J. S. Lee, S. U. Kim, K. Kim, O. Kwon, S. Lee, J. H. Kim, D. S. Lim, Simultaneous measurement of thermal conductivity and interface thermal conductance of diamond thin film, Journal of Vacuum Science and Technology B 27 (2009) 2408–2412.

[15] M. A. Angadi, T. Watanabe, A. Bodapati, X. Xiao, O. Auciello, J. A. Carlisle, J. A. Eastman, P. Keblinski, P. K. Schelling, S. R. Phillpot, Thermal transport and grain boundary conductance in ultrananocrystalline diamond thin films, Journal of Applied Physics 99 (2006) –.

[16] V. Ralchenko, S. Pimenov, V. Konov, A. Khomich, A. Saveliev, A. Popovich, I. Vlasov, E. Zavedeev, A. Bozhko, E. Loubnin, R. Khmelnitskii, Nitrogenated nanocrystalline diamond films: Thermal and optical

properties, Diamond and Related Materials 16 (2007) 2067 – 2073. Proceedings of the Joint International Conference: Nanocarbon and Nanodiamond 2006.

[17] M. Shamsa, S. Ghosh, I. Calizo, V. Ralchenko, A. Popovich, A. A. Balandin, Thermal conductivity of nitrogenated ultrananocrystalline diamond films on silicon, Journal of Applied Physics 103 (2008) –.

[18] T. R. Anthony, J. L. Fleischer, J. R. Olson, D. G. Cahill, The thermal conductivity of isotopically enriched polycrystalline diamond films, Journal of Applied Physics 69 (1991) 8122–8125.

[19] O. Käding, E. Matthias, R. Zachai, H.-J. Füßer, P. Münzinger, Thermal diffusivities of thin diamond films on silicon, Diamond and Related Materials 2 (1993) 1185 – 1190.

[20] E. Bozorg-Grayeli, A. Sood, M. Asheghi, V. Gambin, R. Sandhu, T. I. Feygelson, B. B. Pate, K. Hobart, K. E. Goodson, Thermal conduction inhomogeneity of nanocrystalline diamond films by dual-side thermoreflectance, Applied Physics Letters 102 (2013) –.

[21] K. E. Goodson, O. W. Käding, M. Rösler, R. Zachai, Experimental investigation of thermal conduction normal to diamondsilicon boundaries, Journal of Applied Physics 77 (1995) 1385–1392.

[22] H. Verhoeven, A. Flöter, H. Reiß, R. Zachai, D. Wittorf, W. Jäger, Influence of the microstructure on the thermal properties of thin polycrystalline diamond films, Applied Physics Letters 71 (1997) 1329–1331.

[23] J. Philip, P. Hess, T. Feygelson, J. E. Butler, S. Chattopadhyay, K. H. Chen, L. C. Chen, Elastic, mechanical, and thermal properties of nanocrystalline diamond films, Journal of Applied Physics 93 (2003) 2164–2171.

[24] J. Anaya, S. Rossi, M. Alomari, E. Kohn, L. Tth, B. Pcz, M. Kuball, Thermal conductivity of ultrathin nano-crystalline diamond films determined by

19

raman thermography assisted by silicon nanowires, Applied Physics Letters 106 (2015) –.

[25] K. Janischowsky, W. Ebert, E. Kohn, Bias enhanced nucleation of diamond on silicon (100) in a HFCVD system, Diamond and Related Materials 12 (2003) 336–339.

[26] T. Feygelson, K. Hobart, M. Ancona, F. Kub, J. Butler, Fabrication of silicon-on-diamond (sod) substrates, Meeting Abstracts MA2005-01 (2006) 510.

[27] C. Wild, P. Koidl, W. Mller-Sebert, H. Walcher, R. Kohl, N. Herres, R. Locher, R. Samlenski, R. Brenn, Chemical vapour deposition and characterization of smooth 100-faceted diamond films, Diamond and Related Materials 2 (1993) 158 – 168. Diamond 1992 Proceedings of the Third International Conference on the New Diamond Science and Technology.

[28] O. Williams, Nanocrystalline diamond, Diamond and Related Materials 20 (2011) 621 – 640.

[29] J. Asmussen, D. Reinhard, Diamond films handbook, CRC Press, 2002.

[30] H. Abrams, Grain size measurement by the intercept method, Metallography 4 (1971) 59 – 78.

[31] P. C. Sharma, K. S. Dubey, G. S. Verma, Three-phonon scattering and guthrie's limits for its temperature dependence, Phys. Rev. B 4 (1971) 1306–1313.

[32] J. R. Olson, R. O. Pohl, J. W. Vandersande, A. Zoltan, T. R. Anthony, W. F. Banholzer, Thermal conductivity of diamond between 170 and 1200 k and the isotope effect, Phys. Rev. B 47 (1993) 14850–14856.

[33] J. M. Ziman, Electrons and phonons: the theory of transport phenomena in solids, Oxford University Press, 1960.

[34] J. Callaway, Model for lattice thermal conductivity at low temperatures, Phys. Rev. 113 (1959) 1046–1051.

[35] M. G. Holland, Analysis of lattice thermal conductivity, Phys. Rev. 132 (1963) 2461–2471.

[36] P. Carruthers, Theory of thermal conductivity of solids at low temperatures, Rev. Mod. Phys. 33 (1961) 92–138.

[37] M. Asen-Palmer, K. Bartkowski, E. Gmelin, M. Cardona, A. P. Zhernov, A. V. Inyushkin, A. Taldenkov, V. I. Ozhogin, K. M. Itoh, E. E. Haller, Thermal conductivity of germanium crystals with different isotopic compositions, Phys. Rev. B 56 (1997) 9431–9447.

[38] D. T. Morelli, J. P. Heremans, G. A. Slack, Estimation of the isotope effect on the lattice thermal conductivity of group iv and group iii-v semiconductors, Phys. Rev. B 66 (2002) 195304.

[39] J. A. Krumhansl, Thermal conductivity of insulating crystals in the presence of normal processes, Proceedings of the Physical Society 85 (1965) 921.

[40] P. G. Klemens, The scattering of low-frequency lattice waves by static imperfections, Proceedings of the Physical Society. Section A 68 (1955) 1113.

[41] Y. Kinemuchi, H. Nakano, M. Mikami, K. Kobayashi, K. Watari, Y. Hotta, Enhanced boundary-scattering of electrons and phonons in nanograined zinc oxide, Journal of Applied Physics 108 (2010) –.

[42] E. Wörner, C. Wild, W. Müller-Sebert, R. Locher, P. Koidl, Thermal conductivity of cvd diamond films: high-precision, temperature-resolved measurements, Diamond and Related Materials 5 (1996) 688 – 692. Proceedings of the 6th European Conference on Diamond, Diamond-like and Related Materials Part 2.

[43] K. Belay, Z. Etzel, D. G. Onn, T. R. Anthony, The thermal conductivity of polycrystalline diamond films: Effects of isotope content, Journal of Applied Physics 79 (1996) 8336–8340.

[44] N. Savvides, H. J. Goldsmid, Boundary scattering of phonons in fine-grained hot-pressed ge-si alloys. ii. theory, Journal of Physics C: Solid State Physics 13 (1980) 4671.

[45] W. Li, N. Mingo, L. Lindsay, D. A. Broido, D. A. Stewart, N. A. Katcho, Thermal conductivity of diamond nanowires from first principles, Phys. Rev. B 85 (2012) 195436.

[46] S. Bhattacharyya, O. Auciello, J. Birrell, J. A. Carlisle, L. A. Curtiss, A. N. Goyette, D. M. Gruen, A. R. Krauss, J. Schlueter, A. Sumant, P. Zapol, Synthesis and characterization of highly-conducting nitrogen-doped ultra-nanocrystalline diamond films, Applied Physics Letters 79 (2001) 1441–1443.

[47] S. Dannefaer, W. Zhu, T. Bretagnon, D. Kerr, Vacancies in polycrystalline diamond films, Phys. Rev. B 53 (1996) 1979–1984.

[48] X. Zhou, G. D. Watkins, K. M. McNamara Rutledge, R. P. Messmer, S. Chawla, Hydrogen-related defects in polycrystalline cvd diamond, Phys. Rev. B 54 (1996) 7881–7890.

[49] P. Reichart, G. Datzmann, A. Hauptner, R. Hertenberger, C. Wild, G. Dollinger, Three-dimensional hydrogen microscopy in diamond, Science 306 (2004) 1537–1540.

[50] H. Verhoeven, J. Hartmann, M. Reichling, W. Mller-Sebert, R. Zachai, Structural limitations to local thermal diffusivities of diamond films, Diamond and Related Materials 5 (1996) 1012 – 1016.

[51] D. Twitchen, C. Pickles, S. Coe, R. Sussmann, C. Hall, Thermal conductivity measurements on {CVD} diamond, Diamond and Related Materials

10 (2001) 731 – 735. 11th European Conference on Diamond, Diamond-like Materials, Carbon Nanotubes, Nitrides and Silicon Carbide.

[52] S. K. Estreicher, T. M. Gibbons, M. B. Bebek, Thermal phonons and defects in semiconductors: The physical reason why defects reduce heat flow, and how to control it, Journal of Applied Physics 117 (2015) –.

[53] H. Dong, B. Wen, R. Melnik, Relative importance of grain boundaries and size effects in thermal conductivity of nanocrystalline materials, Scientific Reports 4 (2014) 7037 EP –.

[54] Q. Hao, General effective medium formulation for thermal analysis of a polycrystalthe influence of partially specular phonon transmission across grain boundaries, Journal of Applied Physics 116 (2014) –.

[55] C. Hua, A. J. Minnich, Importance of frequency-dependent grain boundary scattering in nanocrystalline silicon and silicongermanium thermoelectrics, Semiconductor Science and Technology 29 (2014) 124004.

[56] J. E. Graebner, S. Jin, G. W. Kammlott, B. Bacon, L. Seibles, W. Banholzer, Anisotropic thermal conductivity in chemical vapor deposition diamond, Journal of Applied Physics 71 (1992) 5353–5356.

[57] G. Lu, W. T. Swann, Measurement of thermal diffusivity of polycrystalline diamond film by the converging thermal wave technique, Applied Physics Letters 59 (1991) 1556–1558.

[58] J. E. Graebner, S. Jin, G. W. Kammlott, J. A. Herb, C. F. Gardinier, Large anisotropic thermal conductivity in synthetic diamond films, Nature 359 (1992) 401–403.

[59] S. Lani, C. Ataman, W. Noell, D. Briand, N. de Rooij, Thermal characterization of polycrystalline {CVD} diamond thin films, Procedia Chemistry 1 (2009) 609 – 613. Proceedings of the Eurosensors {XXIII} conference.

[60] S. Wolter, D.-A. Borca-Tasciuc, G. Chen, N. Govindaraju, R. Collazo, F. Okuzumi, J. Prater, Z. Sitar, Thermal conductivity of epitaxially textured diamond films, Diamond and Related Materials 12 (2003) 61 – 64.

[61] M. Bertolotti, G. L. Liakhou, A. Ferrari, V. G. Ralchenko, A. A. Smolin, E. Obraztsova, K. G. Korotoushenko, S. M. Pimenov, V. I. Konov, Measurements of thermal conductivity of diamond films by photothermal deflection technique, Journal of Applied Physics 75 (1994) 7795–7798.

[62] O. Käding, M. Rösler, R. Zachai, H.-J. Fßer, E. Matthias, Lateral thermal diffusivity of epitaxial diamond films, Diamond and Related Materials 3 (1994) 1178 – 1182.

[63] Y. Yamamoto, T. Imai, K. Tanabe, T. Tsuno, Y. Kumazawa, N. Fujimori, The measurement of thermal properties of diamond, Diamond and Related Materials 6 (1997) 1057 – 1061.

[64] E. Six, Private communication, 2014.

[65] D. Das, R. N. Singh, S. Chattopadhyay, K. Chen, Thermal conductivity of diamond films deposited at low surface temperatures, Journal of materials research 21 (2006) 2379–2388.

[66] Y. Li, R. Taylor, A. Nabi, Thermal diffusivity measurement of cvd diamond film using a step heating technique, International Journal of Thermophysics 14 (1993) 285–295.

[67] J. Hartmann, M. Costello, M. Reichling, Influence of thermal barriers on heat flow in high quality chemical vapor deposited diamond, Phys. Rev. Lett. 80 (1998) 117–120.

[68] V. Goyal, S. Subrina, D. L. Nika, A. A. Balandin, Reduced thermal resistance of the silicon-synthetic diamond composite substrates at elevated temperatures, Applied Physics Letters 97 (2010) –.

24

[69] C. Ratsifaritana, P. Klemens, Scattering of phonons by vacancies, International Journal of Thermophysics 8 (1987) 737–750.

[70] J. E. Graebner, S. Jin, Thermal properties of optical-quality diamond films (invited paper), Proc. SPIE 1759 (1992) 167–177.

[71] A. Ono, T. Baba, H. Funamoto, A. Nishikawa, Thermal conductivity of diamond films synthesized by microwave plasma cvd, Japanese Journal of Applied Physics 25 (1986) L808.

[72] J. Graebner, V. Ralchenko, A. Smolin, E. Obraztsova, K. Korotushenko, V. Konov, Thermal conductivity of thin diamond films grown from d.c. discharge, Diamond and Related Materials 5 (1996) 693 – 698. Proceedings of the 6th European Conference on Diamond, Diamond-like and Related Materials Part 2.

[73] C. Gu, Z. Jin, X. Lu, G. Zou, J. Zhang, R. Fang, The deposition of diamond film with high thermal conductivity, Thin Solid Films 311 (1997) 124 – 127.
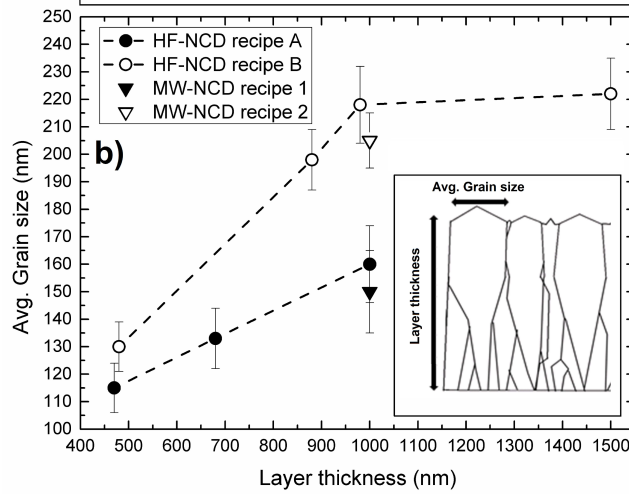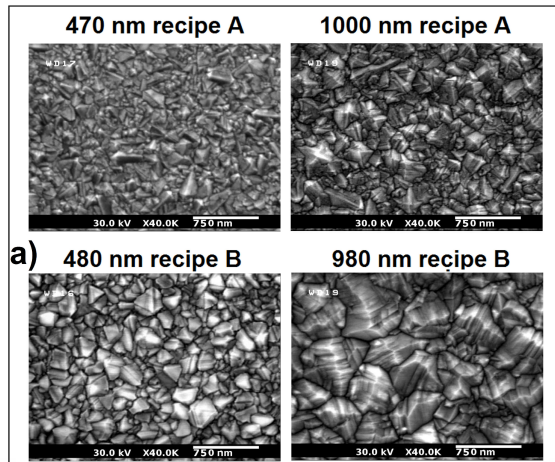
Figure 1: a) Scanning electron microscopy micrographs showing the grain evolution of the HF-NCD. For the same thickness, samples grown with the recipe B show bigger grains than those grown with recipe A. b) Lateral grain size as a function of the thickness for the different NCD films under study. The grain size was extracted by means of the Abrams method[30]. The inset shows a sketch of the typical columnar grain structure of the samples.
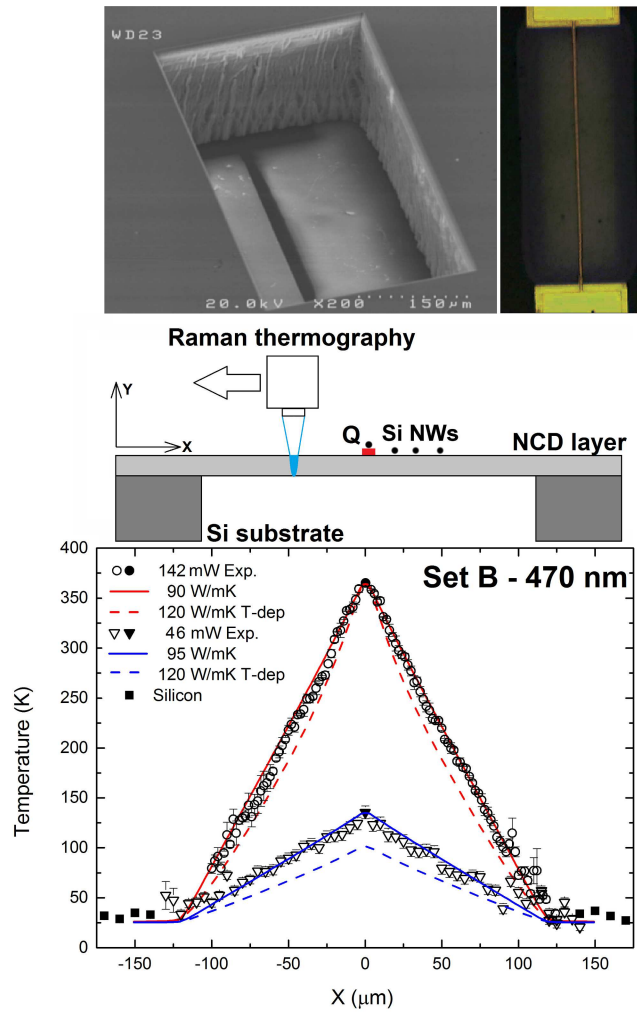
Figure 2: a)-Electron microscopy and optical micrograph of the free standing membranes created for measuring the in-plane thermal conductivity of the diamond films. Note the clear transparency of the diamond films. b) Temperature profiles extracted for the 470 nm thick sample (set B) from the NCD (open symbols) and Si NW (filled circles and triangles) with two different electrical powers dissipated in the heater (142 mW and 46 mW)
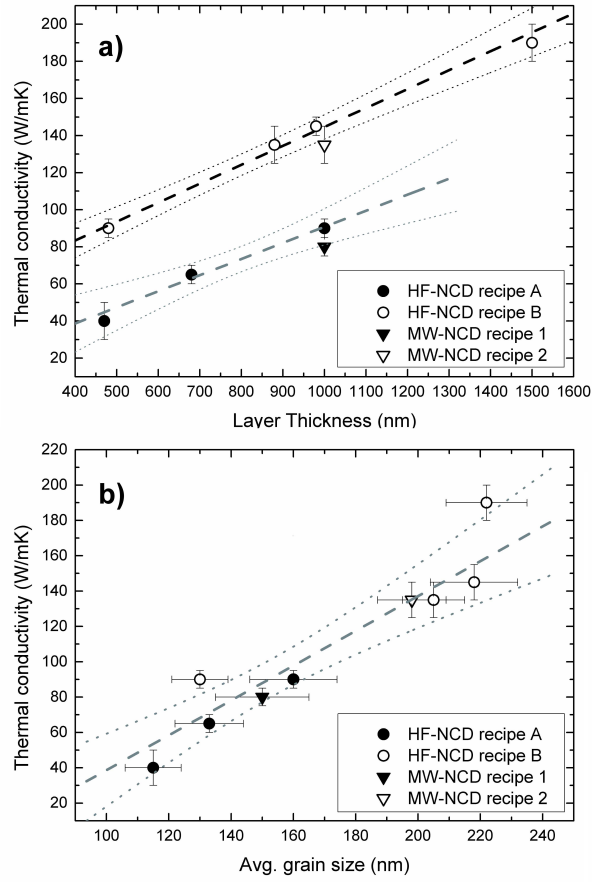
Figure 3: Lateral thermal conductivity measured in the different NCD membranes represented as a function of their layer thickness (a) and lateral grain size at surface (b). Dashed lines corresponds to the least squares linear fitting and dotted lines mark the 90% confidence intervals.
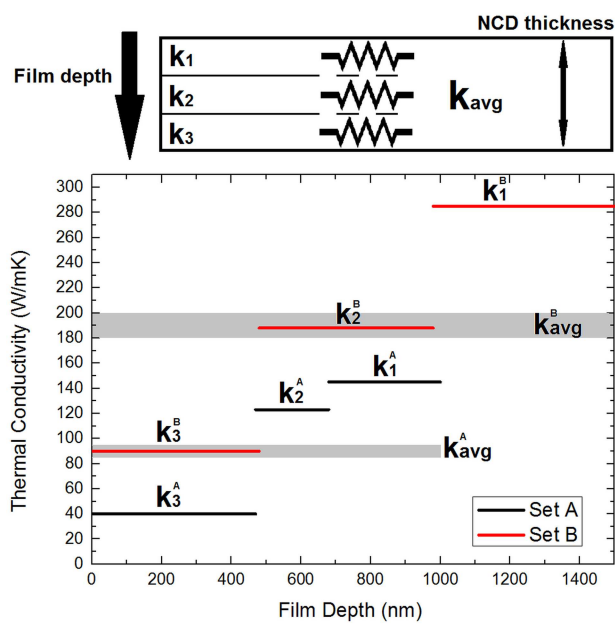
Figure 4: Average thermal conductivity as a function of the depth for the thickest sample of each set (1μ set A and 1.5μm set B) of HF diamond extracted by fitting a multilayer recursive model. The grey bands show the average thermal conductivity measured for the 1μm set A and 1.5μm set B membranes.
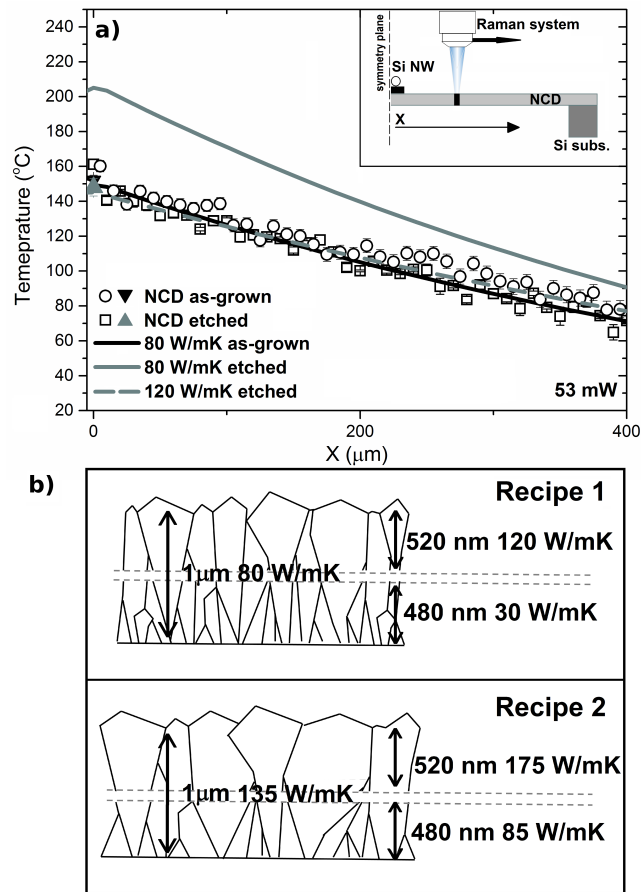
Figure 5: a) Temperature profiles measured in the MW NCD membrane (recipe 1) before and after etching the near nucleation region with the same power dissipated in the heater (temperature measured in the diamond open symbols, Si NW solid symbols). The solid grey curve shows the expected temperature profile assuming that the in-plane thermal conductivity of the etched sample is the same than the one measured in the as-grown sample. b) In-plane thermal conductivity at different depths extracted for the MW-NCD membranes.
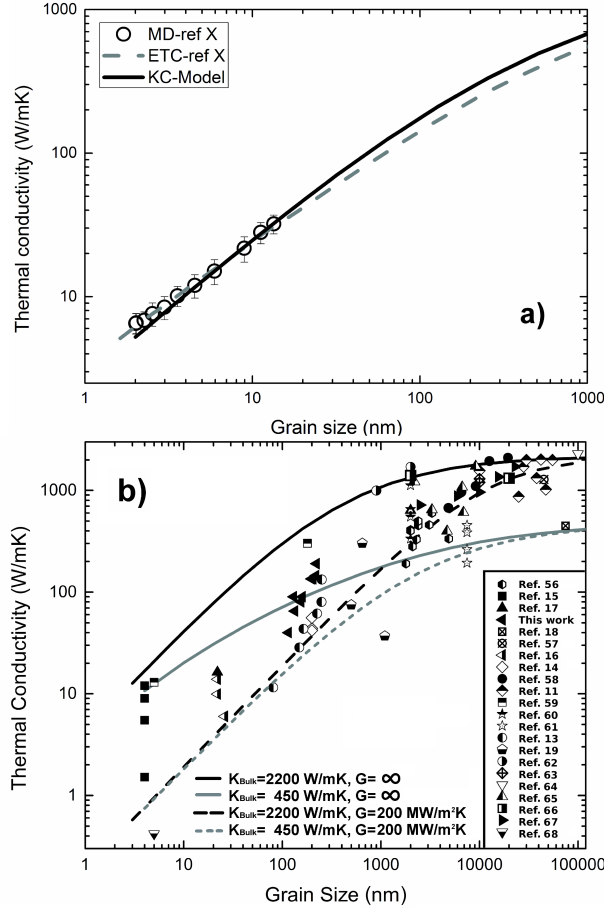
Figure 6: a) Comparison of the KC-model used here and ETC model from [[53]] assuming the same thermal conductance between grains (7 GW/m^2K) and bulk thermal conductivity (1250 W/mK). Results from ab initio molecular dynamics[53] are also shown for comparison. b) Experimental thermal conductivity data versus grain sizes from the literature.[11, 13, 14, 15, 16, 17, 56, 57, 58, 59, 60, 61, 62, 63, 64, 65, 66, 67, 68] Solid curves show the predictions with $G=\infty$ considering natural diamond parameters (black) and lower quality diamond (grey, Γ equivalent to 2500 ppm of C-vacancies). Note that the curves comprise all the data above 1 μm but cannot reproduce the data below 1 μm. By including the thermal barrier between grains the data below 1 μm can be explained (dotted lines).
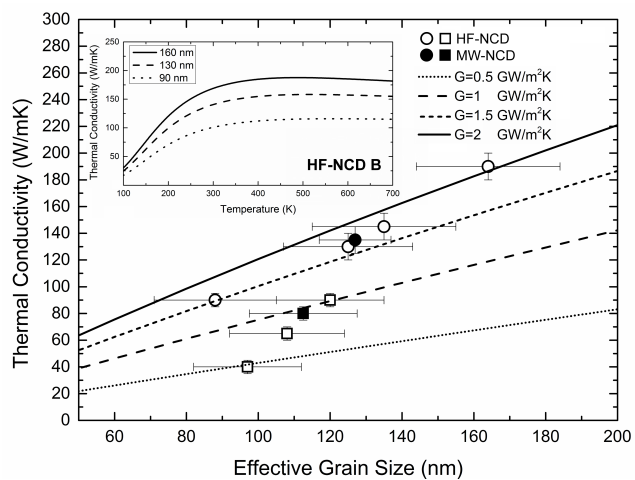
Figure 7: Experimentally in-plane thermal conductivity as a function of the effective grain size determined for each sample. The lines are the result of the model for different values of G. Inset shows the temperature dependence predicted for HF-NCD (recipe B) as an example (G=1.75 GW/m^{2}K). Note the weak temperature dependence of the in-plane thermal conductivity at room temperature and above.
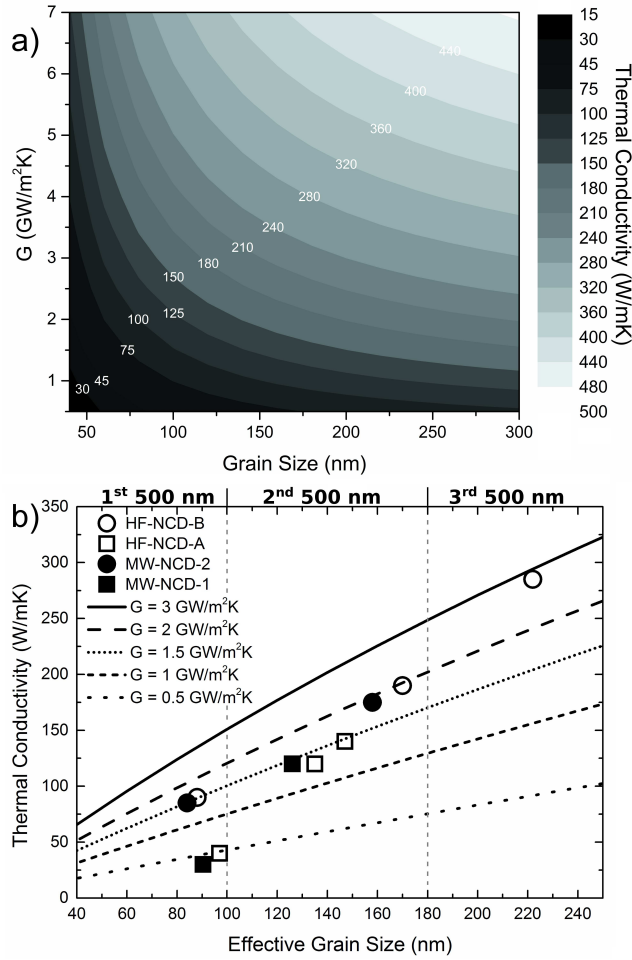
Figure 8: a) Contour plot showing the relative effect of the grain size and G in the thermal conductivity of nanocrystalline diamond. b) Experimentally in-plane thermal conductivity as a function of the effective grain size determined for each region of the films (vertical dashed lines are guides to the eye). The lines are results of the model with the thermal conductance between grains indicated in the graph.